Volume 1 | Number 1 | Jan 2013 | Pages 1–100

# Nanoscale

www.rsc.org/nanoscale

ROYAL SOCIETY OF CHEMISTRY

ROYAL SOCIETY OF CHEMISTRY

www.rsc.org/nanoscale

# Journal Name

## ARTICLE

# Large-scale generation of cell-derived nanovesicles

W. Jo,[a] J. Kim,[b] J. Yoon,[a] D. Jeong,[b] S. Cho,[a] H. Jeong,[a] Y. J. Yoon,[d] S. C. Kim,[c] Y. S. Gho,[d] and J. Park*[ab]

Exosomes are enclosed compartments that are released from cells and that can transport biological contents for the purpose of intercellular communications. Research into exosomes is hindered by their rarity. In this article, we introduce a device that uses centrifugal force and a filter with micro-sized pores to generate a large quantity of cell-derived nanovesicles. The device has a simple polycarbonate structure to hold the filter, and operates in a common centrifuge. The nanovesicles are similar in size and membrane structure to exosomes. The nanovesicles contain intracellular RNAs ranging from micro RNA to mRNA, intracellular proteins, and plasma membrane proteins. The quantity of nanovesicles produced using the device is 250 times the quantity of naturally-secreted exosomes. Also, the quantity of intracellular contents in the nanovesicles is twice that in exosomes. Nanovesicles generated from murine embryonic stem cells can transfer RNAs to target cells. Therefore, this novel device and the nanovesicles that it generates are expected to be used in exosome-related research, and can be applied in various applications such as drug delivery and cell-based therapy.

## Introduction

Exosomes released from eukaryotic cells have important functions in cell-to-cell communication, but their characteristics are not fully understood.[1, 2] Exosomes are 50~200 nm in diameter and are enclosed by a phospholipid bilayer membrane; they contain biological contents of cells from which they originated.[3] Both in functionality and structure, the exosome membrane may be similar to the cell plasma membrane because they are both derived from the endosome.[4] During biogenesis of exosomes, their bilayer is amended with membrane proteins that activate cell surface receptors and initialize signal transduction,[5] and the enclosed sac of the lipid bilayer contains cellular contents such as mRNA, microRNA and cytosolic proteins that can be delivered to recipient cells during cell-to-cell interaction.[6, 7] Due to these abilities to transfer biological contents among recipient cells, exosomes may have use in biomedical applications, such as regenerative medicine and drug delivery.[8-10]

Research on exosomes is difficult because they are released from cells in very small quantities, usually ~0.1 μg (based on membrane protein concentration; Bradford assay) from $10^6$ cells per day.[11] To isolate enough exosomes for research, significant efforts are required, and the purification process is time-consuming and complex.[11-13] A common purification method includes several ultracentrifuge steps for removing cells, debris and soluble proteins. During this lengthy process, a significant portion of exosomes secreted from cells may be lost.[14] One strategy to overcome this shortage is to fabricate cell-derived nanovesicles on a large scale.

Among the currently available technologies, liposomes are similar to exosomes in their topology and purpose; both are small sacs enclosed by a lipid layer that have contents to be delivered to target cells. Liposomes can be easily generated, and their lipid composition can be optimally modulated.[15-17] Also, surface modification can give them structural stability and targeting ability.[15, 18] However, in contrast to exosomes, liposome generation requires several organic solvents and synthetic materials,[16] which may not be compatible with biological systems. Additionally, successful loading of contents such as RNAs and proteins into liposomes is a challenging task.

An alternative approach is to generate cell-derived nanovesicles by extruding cells through microchannels.[19, 20] Given that the nanovesicles mimic exosomes, both the membrane proteins and intercellular contents such as RNAs and proteins in the nanovesicles are critical criteria to evaluate the similarity between the nanovesicles and exosomes. Nanovesicles have been shown to deliver the contained RNAs to target cell.

Although this method is successful in mimicking exosomes, delivery efficiency and scaling-up for applications are practical challenges. The required dose of nanovesicles depends on the concentration of RNA and protein enclosed in the nanovesicles. Typically, both endocytosis and exocytosis of exosomes require cellular energy; for example, exocytosis of one exosome costs about ~25 ATPs,[21] so that a nanovesicle that contains high concentrations of RNAs and proteins should be more effective than one with low concentrations. Also, to make applications of the nanovesicles practical, they should be produced on a large scale with uniform quality under controlled conditions.

In this work, we have developed a scaled-up cell-derived nanovesicle generation system by using common centrifuge that can apply well-controlled force when cells pass through filters with micro-sized pores. When centrifuge operated,

nanovesicles were directly fabricated from cells that were elongated while passing through hydrophilic micro-size pores. The nanovesicles had concentrations of intracellular contents that were double those in exosomes. We also demonstrated that the nanovesicles can deliver their contents to recipient cells and activate signaling pathways. These results suggest that the new nanovesicle generation system can generate effective nanovesicles in large quantities; it is expected to contribute to exosome-related research and applications.

## Experimental

### Device description and nanovesicle generation

A device that uses centrifugal force and a micro-sized polycarbonate filter was designed to generate nanovesicles (Fig. 1a). The device has several mechanical components: a pair of syringes, pistons and caps, a filter holder and a polycarbonate filter. The device has outer height of 120 mm and outer diameter of 28 mm, which are the same as those of a 50 mL tube to fit in the centrifuge bucket (Fig. 1b). For repeating reciprocal processes, the device is symmetrical: two identical extruding units are assembled across the polycarbonate filter. The polycarbonate filter is supported by a filter holder which has several holes of 1 mm diameter. Each syringe can contain up to 5 mL of cell-suspending buffer. When this cell-suspending buffer is loaded into one syringe, the surface tension from the polycarbonate filter prevents the buffer from leaking to the other syringe. To apply force to the piston, a 21 g copper mass was set on the top of the piston. As a result, the angular velocity $\omega$ of centrifuge and the mass of the copper determine the pressure applied to cells during cell extrusion. During extrusion, the polycarbonate filter imposes surface tension and disrupts the cells when they pass through pores (Fig. 1c). The symmetric structure across the polycarbonate filter allows cells to pass through the polycarbonate filter repeatedly. Two O-rings and a polydimethylsiloxane sheet were used to seal the device. To reduce friction between the syringe and the piston surface, silicon lubricant was applied to the inside of the syringe.

### Cell culture

The experiments tested three cell types. Murine embryonic stem cell line D3 (ES cell) was obtained from the American type culture collection (ATCC, CRL-1934). ES cells were cultured in knockout DMEM (Gibco) that included 15% knockout serum (Gibco), 4 mM L-glutamine (Sigma), 100 unit $mL^{-1}$ penicillin-streptomycin (Gibco), 1 μg $mL^{-1}$ leukemia inhibitory factor (ORF genetics), and 0.1 mM 2-mercaptoethanol (Sigma). NIH-3T3 fibroblasts (ATCC, CRL-1658) and Mouse embryonic fibroblasts (MEFs) that expressed Green fluorescence protein (GFP) were cultured in DMEM that included 10% fetal bovine serum (Hyclone) and 100 unit $mL^{-1}$ penicillin-streptomycin (Gibco). MEF-GFP were isolated from a $\beta$-actin mouse (Jackson Laboratories) and used as recipient cells. Isolation from $\beta$-actin mouse was approved by the Institutional Animal Care and Use Committee at POSTECH, Pohang, Republic of Korea (approval number: 2013-01-0016).

### Exosome isolation

ES cells were cultured for 24 h in medium that contained knockout serum whose exosome content was depleted by centrifugation at 150,000 × g at 4 °C for 16 h. To remove cells and debris, the cell culture medium was centrifuged at 500 × g for 10 min, 3000 × g for 20 min and 10,000 × g for 30 min. The supernatant was ultra-centrifuged at 100,000 × g for 100 min to collect the exosomes. The collected exosomes were purified by ultracentrifugation at 150,000 × g for 2 h in a gradient of 35%, 25% and 5% optiprep/tris-HCL.
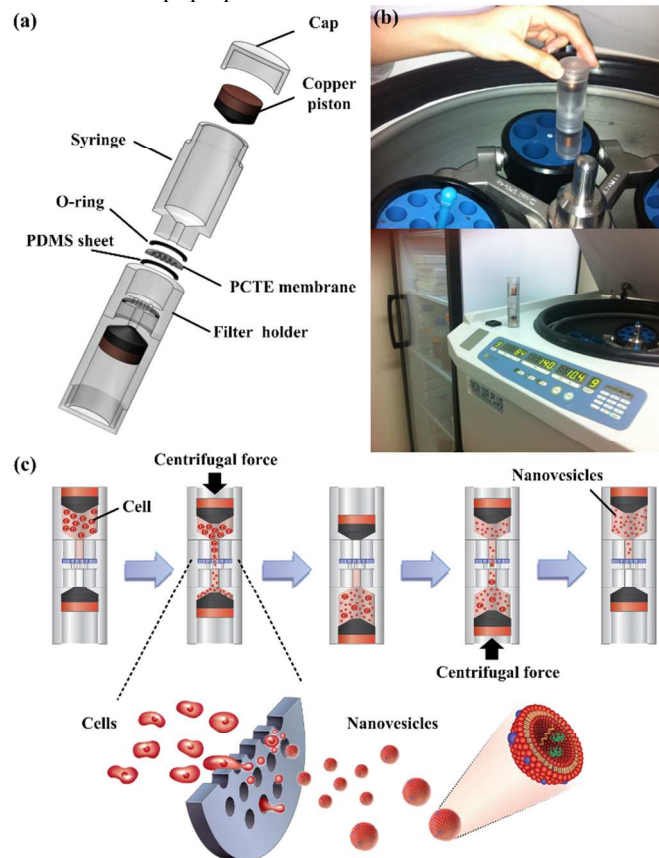


**Fig. 1** (a) Sectional view of device. (b) Photograph of device in operation. (c) Schematic process of nanovesicle generation. After cells were loaded into the syringe, centrifugal force was applied to extrude them. During extrusion, the polycarbonate filter imposes surface tension and generates nanovesicles when they pass through the filter pores.

### Generation of nanovesicles

Nanovesicles were generated from $1 \times 10^8$ ES cells diluted in 1 mL phosphate-buffered saline (PBS). They were extruded three times through both a 10 μm pore polycarbonate track-etched (PCTE) filter (Whatman) and a 5 μm pore PCTE filter (Whatman). The samples were purified by ultracentrifugation at 100,000 × g for 1 h in a gradient of 30% and 10% optiperp/tris-HCl.

### Nanovesicle size measurement

Nanovesicle size was measured using a dynamic scattering laser (ZETASIZER 3000HSA, MALVERN Instrument). Samples that contained 5 μg of either nanovesicles or exosomes

(quantified by Bradford protein assay) were diluted in 1 mL PBS. Each sample was measured three times.

## Quantitative and total protein analysis of exosomes and nanovesicles

The quantities of exosomes and nanovesicles were determined using the Bradford protein assay (Bio-rad) that measures surface protein content. This assay represents the quantity of exosomes and nanovesicles indirectly measuring surface protein of exosome and nanovesicles.

The total protein of exosome and nanovesicle samples were measured using the Bicinchoninic acid (BCA) protein assay kit (Thermo scientific) after they were lysed using Radio-immunoprecipitation assay (RIPA) buffer for 10 min and their lipid were removed by centrifugation at $10,000 \times g$ for 10 min.

## Total RNA isolation from exosomes and nanovesicles

Exosomes and nanovesicles are lysed in tri-reagent (Sigma) for 5 min. The sample was then mixed with chloroform and centrifuged at $13,500 \times g$ for 10 min to separate the organic phase from the aqueous phase. The aqueous phase was collected and mixed with an equal volume of isopropyl alcohol (IPA), held at -20 °C for 20 min, then centrifuged at $13,500 \times g$ for 10 min. The supernatant was removed and 75% ethanol was added to wash away the IPA. The samples were then centrifuged at $13,500 \times g$ for 10 min, then the supernatant was removed and the RNA pellet was dried to remove the ethanol. The RNA pellet was dissolved in nuclease-free water (Ambion).

## Electron microscopy

Exosomes and nanovesicles were imaged using transmission electron microscopy to verify their morphology. Samples of 5 μL volume (400 μg/μL) were prepared and dropped on parafilm. A Formavar carbon film (FCF300-cu, Electron Microscopy Science) was placed on top of each drop and absorbed it. After 5 s, the remaining liquid was removed. For negative staining, the Formavar carbon films were allowed to absorb 2% uranyl acetate for 5 s, then were dried for 30 min at room temperature and imaged using a JEOL transmission electron microscope (JEM-10011, Japan).

## Reverse transcription - polymerase chain reaction

RNAs isolated from exosomes and nanovesicles were quantified using a spectrophotometer (Jenway, Genova). Samples (1 μg) of isolated RNAs were reverse-transcribed using a reverse transcription kit (Promega) at 42 °C for 70 min and 70 °C for 15 min serially. Polymerase chain reaction (PCR) was performed using a polymerase chain reaction kit (Promega) with primers for $\beta$-actin, Oct3/4 and Nanog. The PCR process consisted of denaturation at 94 °C for 2 min, followed by 32 cycles of amplification at 94 °C for 30 s, 52 °C for 30 s, 72 °C for 1 min and extension at 70 °C for 5 min. The mouse $\beta$-actin, Oct 3/4 and Nanog primers used for PCR were:

$\beta$-actin    Forward  ACGTTGACATCCGTAAAGAC
             Reverse  GCAGTAATCTCCTTCTGCAT
Oct 3/4   Forward  AGACCATGTTTCTGAAGTGC
             Reverse  GAACCATACTCGAACCACAT
Nanog    Forward  AGGGTCTGCTACTGAGATGCTCTG
             Reverse  CAACCACTGGTTTTTCTGCCACCG

## Western blot

Cells and nanovesicles were lysed using RIPA buffer with protease inhibitor (Sigma, P8340). Lipid particles were removed by centrifugation at $10,000 \times g$ for 10 min, then total protein was measured using a BCA protein assay kit (Thermo scientific) at 595 nm. Samples (10 μg) of denatured protein (100 °C, 10 min) were loaded and run in 10% SDS-PAGE gel at 100 V for 2 h. Proteins were transferred to a polyvinylidene difluoride membrane and run at 390 mA for 2 h. For blocking, samples were treated with 5% non-fat milk in PBS for 1 h at room temperature, then coated overnight at 4 °C with primary antibody. The samples were coated with secondary antibody for 1 h at room temperature, then proteins were detected using a chemiluminescent substrate (Thermo scientific). The primary antibodies were anti-actin (Santa Cruz, sc-81178), anti-ICAM-1 (biorbyt, orb42646), anti-Nanog (Millipore, SC1000), anti-MAPK p44/42 (Cell Signaling, 9102), anti-phospho MAPK p44/42 (Cell Signaling, 9106); the secondary antibodies were anti-mouse HRP (Santa Cruz); and anti-rabbit HRP conjugated (Santa cruz). Primary antibodies were diluted 1:1000 and secondary antibodies were diluted 1:5000 in 5% non-fat milk in PBS.

## Confocal scanning microscopy

Samples were imaged using a confocal scanning microscope (Olympus, FV1000). ES cells were stained using CellTracker™ Orange CMTMR (Molecular Probes) to generate dyed nanovesicles. As recipient cells, MEF-GFPs were plated on a confocal dish (SPL) coated with 0.2% gelatin (Sigma). After 12 h, MEFs were treated with nanovesicles (10 μg μL$^{-1}$) for 1, 3, 6, or 12 h. Samples were washed in PBS three times and fixed using 4% paraformaldehyde. Nuclei were stained using Hoechst (Sigma). To prevent evaporation, samples were coated with a mounting solution before imaging.

## Results and discussion

### Device operation and optimization

To generate nanovesicles, we fabricated a polycarbonate structure that can embed a PCTE filter. When centrifuge operated, nanovesicles were directly fabricated from cells that were elongated while passing through hydrophilic micro-size pores **(**Fig. 1). The device should be optimized to ensure that cells pass through it at specified with cell numbers and pressures. Murin Embryonic stem (ES) cells were used as source to generate nanovesicles. First, mechanical force was analyzed using our centrifuge (r = 115 mm; Fig. 1b); surface tension of PCTE filter and static friction between polycarbonate surface and piston rubber. When centrifuged, PBS without cells passed through the filter at 600 rpm but not at 500 rpm. Thus, the estimated surface tension that inhibits PBS from passing through the filter was $\sim 0.18$ J·m$^{-2}$. Centrifugal force depressed the piston at 550 rpm but not at 500 rpm, so the estimated static friction between polycarbonate surface and piston rubber was $\sim$ 9.6 N. The smallest pressure required for nanovesicle generation was determined based on the surface tension and the static friction. The required pressure increased as the number $N_c$ of cells increased (Fig. 2a). When $N_c$ exceeded some critical number ($\sim 1 \times 10^8$ for ES cells), no cells passed through the filter at any g-force. Therefore, the condition for highest yield

rate of the nanovesicles from ES cells was set at ~16000 kPa (2000 rpm) and $1 \times 10^8$ ES cells because a large number of cells can make a large number of of nanovesicles.

To determine the conditions required to get nanovesicles of uniform size (measured using DLS), the filter pore size (10 μm, 5 μm) and the number of PCTE filter passes (1, 3, or 5) were controlled. When cells were only passed through a filter with 10 μm pore size, microscopy revealed cell-like particles, because the 10 μm pore is similar to the size of cells; the sample also contained viscous and sticky substances. Although these phenomena decreased as the number of filter passes increased, the nanovesicles were not of uniform size. When cells were only passed through a filter with 5 μm pore size, the generated nanovesicles were of uniform size, but a large proportion of the cells could not pass through the filter in each pass. Although the filter with 10 μm pores cannot be used to generate uniform nanovesicles, it can be used as a pre-filter to help pass a large number of cells through the filter with 5 μm pores. Therefore, 10 μm and 5 μm pore filters were used sequentially to generate nanovesicles.
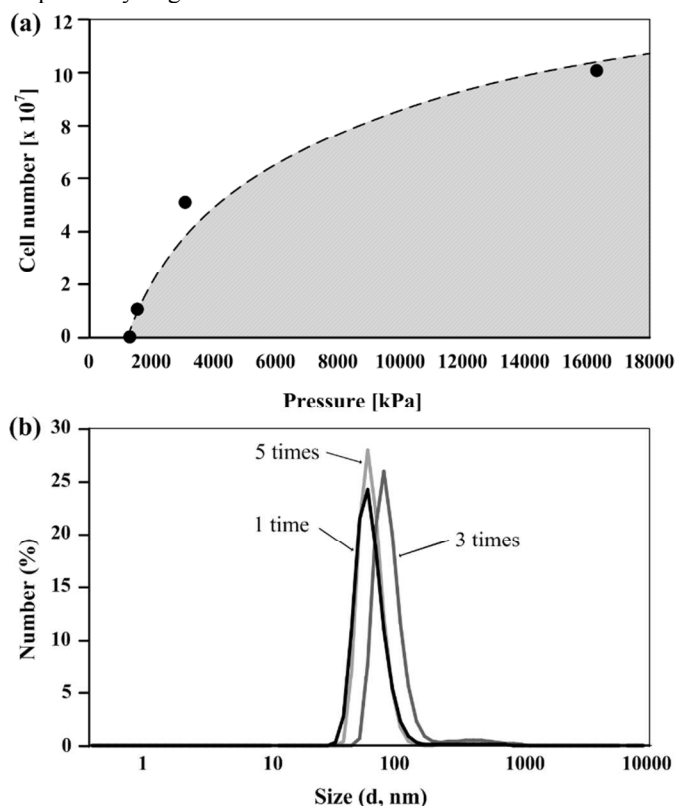


**Fig. 2** (a) Plot of minimum pressure that forces cells to pass through the filter depending on cell number. Pressure required to force cells through the filter increased as cell number increased. (b) The size of nanovesicles generated by passing through 10 μm pore (3 times) and the 5 μm pore filter (1, 3, or 5 times) sequentially. The number of passes does not seem to correlate with the size of nanovesicles.

Also, the number of passes through the PCTE filter was determined for the following reasons. The number of passes should be odd because the non-passed cells could remain on the wall and the bottom of loading syringe. The nanovesicles were generated by passing through the 10 μm pore (3 times) and the 5 μm pore filter (1, 3, or 5 times). When cells passed through the 10 μm pore filter once, the viscous and sticky substance

became stuck in the 5 μm pore filter and blocked it. Therefore, three was chosen as the number of passes through the 10 μm pore filter. The nanovesicles from each sample had uniform diameter (~ 100 nm) (Fig. 2b). The number of passes did not affect the size distributions of nanovesicles, but three filter passes were enough to generate uniform-sized nanovesicles.

**Nanovesicle generation**

The cells that pass through the PCTE membrane filter by centrifugal force should experience tension like cells that pass through a microchannel, due to the similar geometry and surface properties of the two devices.[19] Living cells have a plasma membrane that consists of many components, including lipids, cholesterol, and membrane proteins. The cells are forced down by centrifugal force and driven into the micro-sized pores on the PCTE membrane filter. This PCTE filter coated with Polyvinylpyrrolidone (PVP) (contact angle 42°)[22] had hydrophilic properties, micro-sized pores and 15 μm thickness.

When a cell passes through the pores, the surface of its plasma membrane is extended by adhesive tension caused by friction force between it and the polycarbonate surface of filter because both lipid heads and PVP are hydrophilic and contact each other. The tension makes the plasma membrane elongate mechanically as demonstrated using the micropipette suction method.[23] When the strain and stress exceed a yield point, the lipid bilayer undergoes plastic deformation and even fails (ruptures).[24] For a surface-isotropic material, mean tension $\bar{\tau}$ [J/m$^2$] is proportional to the fractional area dilation $\alpha$:

$$\bar{\tau} = K\alpha; \bar{\tau} \cong \frac{\tau_1 + \tau_2}{2}, \tag{1}$$

where $K$ is the surface compressibility modulus, and $\tau_1$ and $\tau_2$ are principal tensions for orthogonal directions (Fig. 3a). Also, the tension can be changed to pressure difference $P$ across the PCTE membrane:

$$P = \bar{\tau}\left(2 - 2\frac{R_p}{R_c}\right)/R_p, \tag{2}$$

where $R_p$ and $R_c$ are the diameters of a pore and a cell respectively. The order of ultimate tensile strength for failure is ~0.01 mN cm$^{-1}$,[24] so the pressure required to induce membrane failure is on the order of ~(100 Pa) x (number of pores). The pressure was measured using centrifugation; when $\omega$ was 2000 rpm, failure occurred at ~(179 Pa) x (number of pores), which is on the same order as the theoretically estimated value.

The lipid bilayer fragments would be planar immediately after membrane failure, but would immediately self-assemble spontaneously into spheres due to the amphiphilic property of lipids in aqueous solution.[25, 26] To analyze the spontaneous self-assembly using the free energy of thermodynamic stability, we assumed that the planar lipid bilayer is an isotropic homogeneous phospholipid, and that the centerline of the bilayer is rigid and is regarded as an arc of circle with radius $R$ because a lipid bilayer is incompressible along the lateral direction. Although these assumptions are invalid for the lipid bilayer from a plasma membrane, they facilitate analysis of the spontaneous self-assembly. The length of the membrane $L = R\theta$, where $\theta$ is the angle made by the arc (Fig. 3a). The total free energy $G_{total}$ [J] is the sum of energy $G_{bending}$ due to bending and energy $G_{load}$ due to load and can be expressed as

$$G_{total} = G_{bend} + G_{load} = \frac{\kappa_b}{2}\frac{\theta^3}{L} - fL\left(1 - \frac{2}{\theta}\sin\frac{\theta}{2}\right), \qquad (3)$$

where $\kappa_b$ is the bending rigidity and $f$ is line tension.[21, 27] To determine the absolute minimum $\theta$ that is stable thermodynamically, we numerically solved the derivative of Equation 3 with respect to $\theta$:

$$\frac{\partial G_{total}}{\partial \theta} = 0; \theta^3 + \delta\left(\theta\cos\frac{\theta}{2} - 2\sin\frac{\theta}{2}\right) = 0, \qquad (4)$$

where $\delta = fL^2/\kappa_b$. The solution of Equation 4 is varies with $\delta$; when $\delta < 12$, local minima and the absolute minimum of $\theta = 0$; when $\delta > 12$, the absolute minimum of $\theta > 0$. Using experimental values, the bent configuration is spontaneously favored due to minimization of $G_{total}$ when $\sim 20 \le \delta \le \sim 30$.[28, 29] The assumption that the lipid bilayer is isotropic results in the conclusion that the planar bilayer should form a hollow sphere. Therefore, the shredded lipid bilayers in aqueous solution transform into spheres, *i.e.*, nanovesicles. As predicted, the lipid bilayers transformed to spherical nanovesicles enclosed by a lipid bilayer (Fig. 3b) that were similar to exosomes (Fig. 3c) in size and shape.
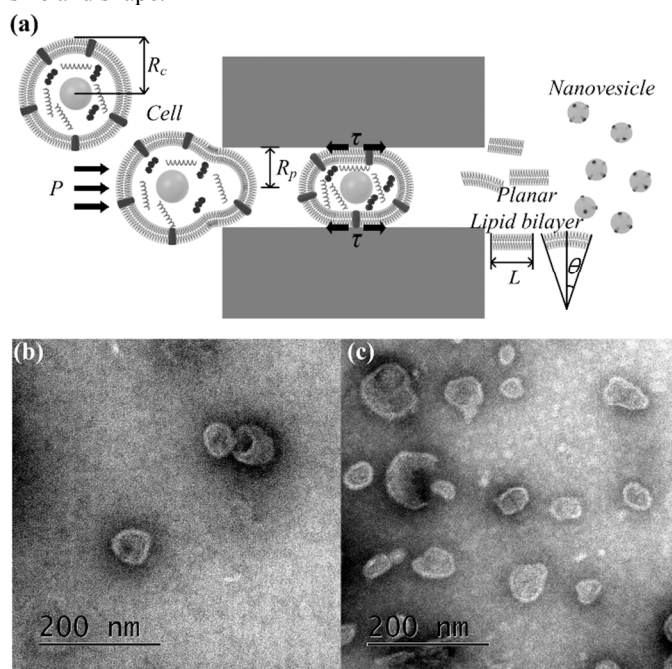
**(a)**



**Fig. 3** (a) Schematic of nanovesicle generation. When a cell passes through a pores, the area of lipid bilayer is extended by the tension caused by adhesion. The tension makes the lipid bilayer elongate, undergo plastic deformation and possibly fail. The lipid bilayers would be a planar form right after the failure, but should spontaneously self-assemble into hollow spheres. TEM image of (b) nanovesicles and (c) exosomes; both are enclosed by a lipid bilayer and have similar structure.

### Quality and efficiency of nanovesicles in various condition

The quantity and quality of nanovesicles were compared at various generation conditions, because force applied to cells differed according to cell population and $\omega$. The equivalent volume of ES cell suspension was prepared with various populations ($1 \times 10^7$, $5 \times 10^7$, and $1 \times 10^8$). The minimum angular velocity $\omega_{min}$ at which cells can pass through the filter increases with cell population, so $\omega$ was set higher than $\omega_{min}$.

These cell suspensions passed through the filter and nanovesicles were generated at $\omega_{min} = 550$, 1000, and 2000 rpm for initial cell populations of $1 \times 10^7$, $5 \times 10^7$, and $1 \times 10^8$ respectively.

The quantity of generated nanovesicles increased linearly as the initial cell population increased (Fig. 4a). Also, the quality (cytosolic contents) of nanovesicles increased as the cell population increased: nanovesicles from $5 \times 10^7$ (1000 rpm) and $1 \times 10^8$ (2000 rpm) samples had ~1.5 times more proteins (Fig. 4b) and ~ 2 times more total RNAs (Fig. 4c) than the nanovesicles from the $1 \times 10^7$ (550 rpm) sample. This result shows that the quantity of cytosolic contents in the nanovesicles increases as the cell population increases. The $1 \times 10^8$ (2000 rpm) condition was chosen for further experiments among various conditions, because this condition gave the highest yield rate of nanovesicles and highest cytosolic contents.

The generation efficiency was verified by comparing the total amount of proteins and RNAs in ES cells and nanovesicles from same number of ES cells. At the chosen conditions, approximately one-sixth of the ES cells changed to nanovesicles (Fig. 4d and e). This proportion was low because many cells became trapped in the filter.
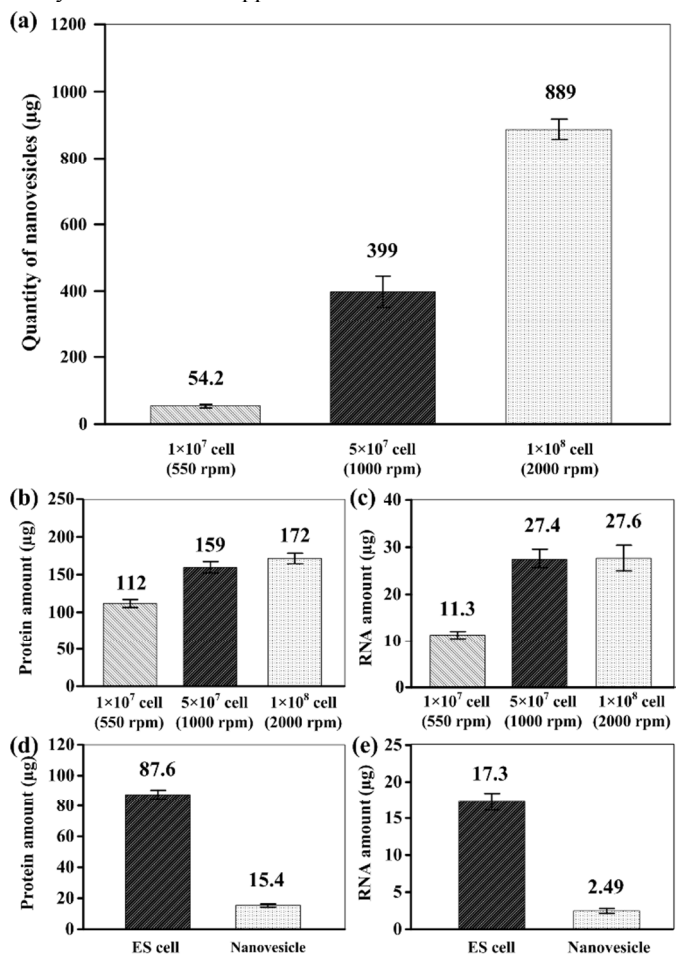


**Fig. 4** (a) Quantity of nanovesicles generated at various initial cell populations and minimum angular velocities. (b) Total protein amount and (c) RNA amount from the equivalent quantity of nanovesicles (100 μg) at various initial cell populations and minimum angular velocities. (d) Total protein amount and (e) RNA amount for $1 \times 10^8$ ES cells and nanovesicles generated from $1 \times 10^8$ ES cells.

## Characteristic of nanovesicles

The characteristics of the nanovesicles were compared in various ways to exosomes and ES cells. Nanovesicles generated from ES cells were ~100 nm in diameter (Fig. 5a), which is similar to the diameter of exosomes (40 ~ 200 nm). Most nanovesicles were spherical, ~100 nm in diameter, and enclosed by a lipid bilayer (Fig. 3b); therefore the products of lipid disruption were nanovesicles, and not nano-particles or debris, and the nanovesicles have a shape similar to that of exosomes, which are also enclosed by a lipid bilayer plasma membrane.
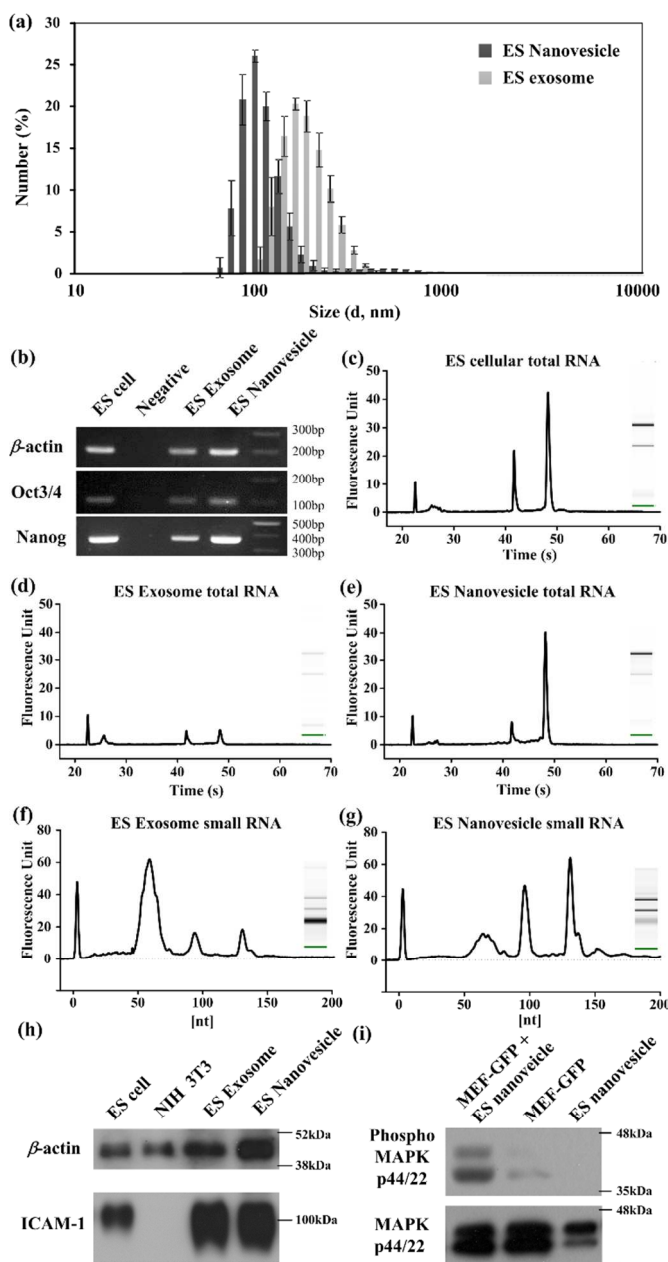


**Fig. 5.** (a) Sizes of nanovesicles generated by $1 \times 10^8$ ES cells and exosome from ES cells, measuring by DLS. (b) Reverse transcription-PCR for ES cells, exosomes, and nanovesicles generated by $1 \times 10^8$ ES cells. Total RNA profiles from Bioanalyzer™ from (c) ES cells, (d) exosomes and (e)

nanovesicles generated by $1 \times 10^8$ ES cells. Small non-coding RNA (25-30 s), mRNA (25-50 s), and rRNA (43 s, 48 s) were detected. Small RNA profiles from (f) ES exosomes and (g) nanovesicles. Micro RNA (25-40 nt), tRNA (50-80 nt) and small rRNA (90-150 nt) were detected. Western blot results for (h) $\beta$-actin (cytosolic protein) and ICAM-1 (membrane protein), (i) Mitogen-activated protein kinase (MAPK) p42/44 (bottom: native form; top: phosphorylated form).

Contents of the ES cells, exosomes, and nanovesicles were analyzed by reverse transcription-PCR, quality analysis of RNA, and western blotting. Housekeeping genes of $\beta$-actin and specific pluripotent markers of Oct3/4[30] and Nanog[31] were expressed by ES-D3 cells, exosomes, and nanovesicles (Fig. 5b). tRNA, rRNA, and microRNA were detected in the ES cells, exosomes, and nanovesicles using Bioanalyzer ™ (Fig. 5c-e). Total RNA profiles of ES cells, exosomes, and nanovesicles were similar. All RNA profiles had three peaks (small RNA and two rRNA), but the RNA profile of ES exosomes had relatively enriched small RNA peak than the other RNA peaks. The small RNA (< 200 nt) was analyzed to check the small RNAs in detail, because the micro RNA, tRNA, and small rRNA cannot be distinguished using total RNA analysis. According to the analysis, both ES exosomes and nanovesicles had same three small RNA peaks (~60 nt, ~100 nt, and ~130 nt), but RNA intensities of ES nanovesicles were different from that of ES exosomes (Fig. 5 f-g). Despite of different RNA quantities, both ES exosomes and nanovesicles consists of same types of RNA. Both reverse transcription-PCR and RNA profile results suggest that the intracellular RNA from the source cells can be conserved and encapsulated in the nanovesicles because nanovesicles were mechanically generated from ES cells without any other treatment. Most cellular contents would be randomly encapsulated in the nanovesicles but specific cellular contents such as small RNAs are non-randomly enriched in exosomes.[6]
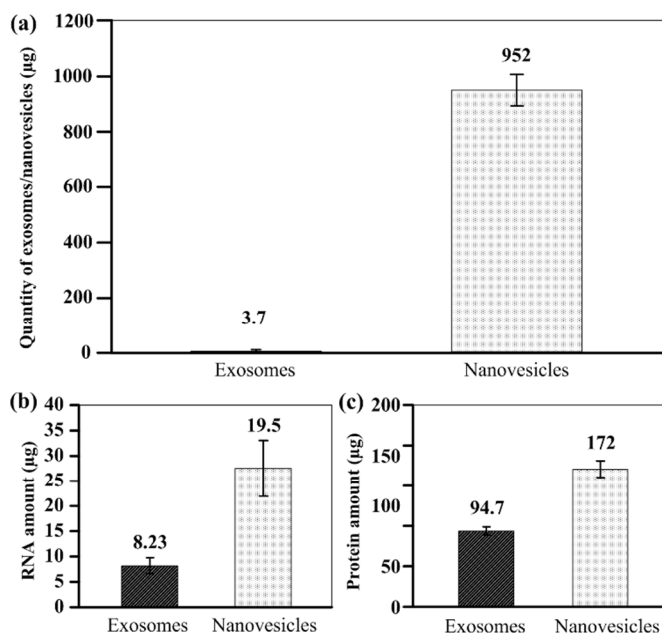


**Fig. 6** (a) Quantity of exosomes and nanovesicles generated from the same number of ES cells ($1 \times 10^8$), measuring by Bradford assay. (b) Total protein amount and (c) RNA amount

were measured from the equivalent amount of exosomes (100 µg) and nanovesicles (100 µg).

Western blotting (Fig. 5f) verified that the nanovesicles express cytosolic proteins (β-actin) and membrane proteins (ICAM-1)[32, 33] as do original cells and exosomes. This result suggests that the contents and lipid bilayer of nanovesicles come from the original cells. Exosomes can activate phosphoylation of Mitogen-activated protein kinase (MAPK),[7] which is an important signaling pathway; for example, they regulate proliferation of mammalian cells.[34] We verified that nanovesicles also activate MAPK phosphoylation on target cells. Nanovesicles (40 µg) were applied for 10 min to MEFs that expressed GFP; after this treatment, Nanovesicle-treated MEF-GFP showed strong band; non-treated MEF-GFP showed weak band; but the nanovesicles did not (Fig. 5g). That is, the nanovesicles contribute to MAPK phopholylation of the target cells. All of these results suggest that the nanovesicles contain intracellular contents,as do exosomes, and can be used to deliver RNA or cytosolic proteins.

### Quality comparison of nanovesicles and exosomes

Cells secrete a small quantity of exosomes (*e.g.*, ~ 0.1 µg from $10^6$ dendritic cells).[11] This small quantity limits applications of exosomes. One of goals of this study was to generate cell-derived nanovesicles efficiently on a large scale. Using the device, a large quantity of nanovesicles can be generated from ES cells. About 250 times more nanovesicles than exosomes were produced from $1 \times 10^8$ ES cells (Fig. 6a). Production efficiency is higher for nanovesicle than for exosomes, because a large portion of cells formed nanovesicles when passed serially through the filter but a small portion of cells formed exosomes.

Also, the total amounts of RNA and protein in equivalent amounts of nanovesicles (100 µg) and exosomes (100 µg) were compared because the amounts of total RNAs and proteins are proportional to the quantity of exosomes.[35, 36] Compared to exosomes, nanovesicles contained about twice as much RNA (Fig. 6b) and twice as much protein (Fig. 6c). These differences may be due to their different generation mechanisms: exosomes were spontaneously released from cells and therefore contain specific intracellular contents, whereas nanovesicles were fabricated from the pieces of plasma membranes of disrupted cells; during self-assembly into vesicles, these membrane fragments would incorporate any contents suspended in the medium that they encapsulated, so the resulting nanovesicles would contain a non-selective set of intracellular contents. Both the high generation efficiency and high quantify of intracellular contents could make the nanovesicles useful as delivery carriers. Typically, in terms of delivery ability, nanovesicles that contain high concentrations of intracellular contents are more effective than those with low concentration because endocytosis and exocytosis require cellular energy; for example, exocytosis of one exosome costs about ~25 ATPs.

### Uptake of nanovesicles

Exosomes can be internalized and deliver their contents to target cells.[10, 36, 37] To verify that the cell-derived nanovesicles can be internalized into target cells, dyed ES nanovesicles were generated, then applied (15 µg) to MEF-GFP cells. Dyed ES nanovesicles penetrated the plasma membranes of the target

cells, and the number that did so increased with treatment duration (Fig. 7a).

Nanovesicles can also deliver their intracellular contents (from original cells) to other types of cells. NIH 3T3 fibroblast were treated with equivalent quantity of ES nanovesicles (50 µg) or with ES exosomes (50 µg) every 2 d to compare their delivery ability. After 5 d, treated samples were washed and total RNAs were isolated. Mouse ES specific RNAs (Oct3/4 and Nanog) were detected in cells treated with nanovesicles and exosomes but not in untreated cells (Fig. 7b). These two results confirm that nanovesicles can be internalized and deliver cellular contents which came from source cells to target cells through the plasma membrane. That is, the nanovesicles could be used to deliver biotherapeutic agents synthesized in cells.
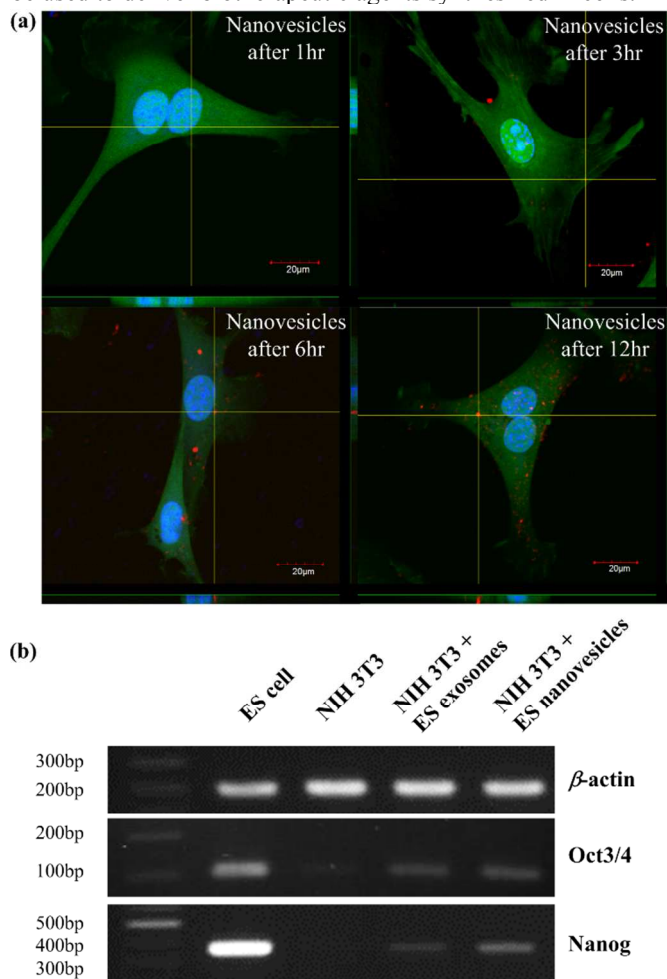


**Fig. 7** (a) Confocal images taken 1, 3, 6, and 12 h after treatment of MEF-GFP (green) with 15 µg of ES nanovesicles (red). (b) Reverse transcription-PCR of ES cells, NIH 3T3 fibroblast, and NIH 3T3 fibroblast treated with ES nanovesicles (50 µg) every 2 d.

### Conclusions

We developed a device that can generate large numbers of cell-derived nanovesicles generation using a common centrifuge and a simple polycarbonate structure that can embed a PCTE filter. Centrifuging a suspension of cells caused them to elongate and rupture while passing through micro-size pores; the resulting cell-membrane fragments self-assembled into spherical nanovesicles with diameters ~100 nm that were

enclosed by a lipid bilayer like exosomes that are secreted by cells. These nanovesicles contained intracellular contents such as cytosolic proteins, RNAs and membrane proteins; this characteristic enabled them to deliver their contents such as Oct 3/4 and Nanog to other cells and to activate Mitogen-activated protein kinase (MAPK) p42/44, which is an important signaling pathway. Furthermore, the concentrations of intracellular contents in the nanovesicles were twice as high as those in exosomes. The new device generated large quantities of nanovesicles that can be used as delivery carriers; it is expected to contribute to research on exosomes and drug delivery systems.

## Acknowledgements

## Notes and references

[a] Department of Mechanical Engineering, POSTECH, 77 Cheongam-Ro, Nam-Gu, Pohang, Gyeongbuk, 790-784, Republic of Korea. E-mail: jpark@postech.ac.kr; Fax: +82 54 279 5899; Tel: +82 54 279 5418

[b] School of Interdisciplinary Bioscience and Bioengineering, POSTECH, 77 Cheongam-Ro, Nam-Gu, Pohang, Gyeongbuk, 790-784, Republic of Korea. E-mail: jpark@postech.ac.kr; Fax: +82 54 279 5899; Tel: +82 54 279 2188

[c] Department of Hepatobiliary & Pancreatic Surgery, Ulsan University College of Medicine and Asan Medical Center, Poongnap-dong, Songpa-gu, Seoul 138-736, Republic of Korea.

[d] Department of Life Science, POSTECH, 77 Cheongam-Ro, Nam-Gu, Pohang, Gyeongbuk, 790-784, Republic of Korea.

1    S. Keller; M. P. Sanderson; A. Stoeck; P. Altevogt, *Immunology letters* 2006, **107** 2, 102-108.
2    E. van der Pol; A. N. Boing; P. Harrison; A. Sturk; R. Nieuwland, *Pharmacol Rev* 2012, **64** 3, 676-705. DOI 10.1124/pr.112.005983.
3    C. Théry; M. Ostrowski; E. Segura, *Nature Reviews Immunology* 2009, **9** 8, 581-593.
4    C. Théry; L. Zitvogel; S. Amigorena, *Nature Reviews Immunology* 2002, **2** 8, 569-579.
5    G. Camussi; M.-C. Deregibus; S. Bruno; C. Grange; V. Fonsato; C. Tetta, *American journal of cancer research* 2011, **1** 1, 98.
6    H. Valadi; K. Ekström; A. Bossios; M. Sjöstrand; J. J. Lee; J. O. Lötvall, *Nature cell biology* 2007, **9** 6, 654-659.
7    J. Ratajczak; K. Miekus; M. Kucia; J. Zhang; R. Reca; P. Dvorak; M. Ratajczak, *Leukemia* 2006, **20** 5, 847-856.
8    J. A. Cho; D. J. Yeo; H. Y. Son; H. W. Kim; D. S. Jung; J. K. Ko; J. S. Koh; Y. N. Kim; C. W. Kim, *International journal of cancer. Journal international du cancer* 2005, **114** 4, 613-22. DOI 10.1002/ijc.20757.
9    S. M. van Dommelen; P. Vader; S. Lakhal; S. Kooijmans; W. W. van Solinge; M. J. Wood; R. M. Schiffelers, *Journal of Controlled Release* 2012, **161** 2, 635-644.
10    L. Alvarez-Erviti; Y. Seow; H. Yin; C. Betts; S. Lakhal; M. J. Wood, *Nat Biotechnol* 2011, **29** 4, 341-5. DOI 10.1038/nbt.1807.
11    C. Thery; S. Amigorena; G. Raposo; A. Clayton, *Current protocols in cell biology / editorial board, Juan S. Bonifacino ... [et al.]* 2006, **Chapter 3**, Unit 3 22. DOI 10.1002/0471143030.cb0322s30.
12    R. T. Davies; J. Kim; S. C. Jang; E. J. Choi; J. Park, *Lab on a Chip* 2012.
13    C. Chen; J. Skog; C.-H. Hsu; R. T. Lessard; L. Balaj; T. Wurdinger; B. S. Carter; X. O. Breakefield; M. Toner; D. Irimia, *Lab on a chip* 2010, **10** 4, 505-511.
14    H. G. Lamparski; A. Metha-Damani; J.-Y. Yao; S. Patel; D.-H. Hsu; C. Ruegg; J.-B. Le Pecq, *Journal of immunological methods* 2002, **270** 2, 211-226.
15    V. P. Torchilin, *Nature Reviews Drug Discovery* 2005, **4** 2, 145-160.
16    A. Sharma; U. S. Sharma, *International Journal of Pharmaceutics* 1997, **154** 2, 123-140.
17    K. Egbaria; N. Weiner, *Advanced drug delivery reviews* 1990, **5** 3, 287-300.
18    J. W. Park; K. Hong; D. B. Kirpotin; G. Colbern; R. Shalaby; J. Baselga; Y. Shao; U. B. Nielsen; J. D. Marks; D. Moore, *Clinical Cancer Research* 2002, **8** 4, 1172-1181.
19    W. Jo; D. Jeong; J. Kim; S. Cho; S. C. Jang; C. Han; J. Y. Kang; Y. S. Gho; J. Park, *Lab on a Chip* 2014, **14** 7, 1261-1269. DOI Doi 10.1039/C3lc50993a.
20    S. C. Jang; O. Y. Kim; C. M. Yoon; D. S. Choi; T. Y. Roh; J. Park; J. Nilsson; J. Lotvall; Y. K. Kim; Y. S. Gho, *ACS Nano* 2013, **7** 9, 7698-710. DOI 10.1021/nn402232g.
21    R. B. Phillips; J. Kondev; J. Theriot; N. Orme; H. Garcia, *Physical biology of the cell*. Garland Science New York: **2009**.
22    L. Kessler; G. Legeay; A. Coudreuse; P. Bertrand; C. Poleunus; X. V. Eynde; K. Mandes; P. Marchetti; M. Pinget; A. Belcourt, *Journal of Biomaterials Science, Polymer Edition* 2003, **14** 10, 1135-1153.
23    A. Roux; G. Koster; M. Lenz; B. Sorre; J.-B. Manneville; P. Nassoy; P. Bassereau, *Proceedings of the National Academy of Sciences* 2010, **107** 9, 4141-4146.
24    E. Evans; D. Needham, *Journal of Physical Chemistry* 1987, **91** 16, 4219-4228.
25    J. N. Israelachvili; D. J. Mitchell; B. W. Ninham, *J. Chem. Soc., Faraday Trans. 2* 1976, **72**, 1525-1568.
26    J. N. Israelachvili; D. J. Mitchell; B. W. Ninham, *Biochimica et Biophysica Acta (BBA)-Biomembranes* 1977, **470** 2, 185-201.
27    Z. Tu, *arXiv preprint arXiv:1212.5673* 2012.
28    M. Antonietti; S. Förster, *Advanced Materials* 2003, **15** 16, 1323-1333.
29    T. Le; U. Olsson; K. Mortensen, *Physica B: Condensed Matter* 2000, **276**, 379-380.
30    M. H. Rosner; M. A. Vigano; K. Ozato; P. M. Timmons; F. Poirie; P. W. Rigby; L. M. Staudt, *Nature* 1990, **345** 6277, 686-692.
31    K. Mitsui; Y. Tokuzawa; H. Itoh; K. Segawa; M. Murakami; K. Takahashi; M. Maruyama; M. Maeda; S. Yamanaka, *cell* 2003, **113** 5, 631-642.
32    P. J. Fairchild; F. A. Brook; R. L. Gardner; L. Graca; V. Strong; Y. Tone; M. Tone; K. F. Nolan; H. Waldmann, *Current Biology* 2000, **10** 23, 1515-1518.
33    L. Tian; J. W. Catt; C. O'Neill; N. King, *Biology of reproduction* 1997, **57** 3, 561-568.
34    W. Zhang; H. T. Liu, *Cell research* 2002, **12** 1, 9-18.
35    A. Savina; M. Furlán; M. Vidal; M. I. Colombo, *Journal of Biological Chemistry* 2003, **278** 22, 20083-20090.
36    A. Montecalvo; A. T. Larregina; W. J. Shufesky; D. B. Stolz; M. L. Sullivan; J. M. Karlsson; C. J. Baty; G. A. Gibson; G. Erdos; Z. Wang, *Blood* 2012, **119** 3, 756-766.
37    A. E. Morelli; A. T. Larregina; W. J. Shufesky; M. L. Sullivan; D. B. Stolz; G. D. Papworth; A. F. Zahorchak; A. J. Logar; Z. Wang; S. C. Watkins, *Blood* 2004, **104** 10, 3257-3266.

**Nanoscale Accepted Manuscript**